SAND2017-7034J

# Next Generation Molten NaI Batteries for Grid Scale Energy Storage

Leo J. Small[a,*], Alexis Eccleston[b], Joshua Lamb[a], Andrew C. Read[b], Matthew Robins[b], Thomas Meaders[b], David Ingersoll[a], Paul G. Clem[a], Sai Bhavaraju[b], Erik D. Spoerke[a]

[a] *Sandia National Laboratories, Albuquerque, NM, USA*

[b] *Ceramatec Inc., Salt Lake City, UT, USA*

**Abstract**

Robust, safe, and reliable grid-scale energy storage continues to be a priority for improved energy surety, expanded integration of renewable energy, and greater system agility required to meet modern dynamic and evolving electrical energy demands. We describe here a new sodium-based battery based on a molten sodium anode, a sodium iodide/aluminum chloride ($NaI/AlCl_3$) cathode, and a high conductivity NaSICON ($Na_{1+x}Zr_2Si_xP_{3-x}O_{12}$) ceramic separator. This NaI battery operates at intermediate temperatures (120-180 °C) and boasts an energy density of >150 Wh $kg^{-1}$. The energy-dense NaI-$AlCl_3$ ionic liquid catholyte avoids lifetime-limiting plating and intercalation reactions, and the use of earth-abundant elements minimizes materials costs and eliminates economic uncertainties associated with lithium metal. Moreover, the inherent safety of this system under internal mechanical failure is characterized by negligible heat or gas production and benign reaction products (Al, NaCl). Scalability in design is exemplified through evolution from 0.85 to 10 Ah (28 Wh) form factors, displaying lifetime average Coulombic efficiencies of 99.45% and energy efficiencies of 81.96% over dynamic testing lasting >3000 hours. This demonstration promises a safe, cost-effective, and long-lifetime technology as an attractive can-

*Corresponding author, Sandia National Laboratories, PO Box 5800, MS 1411, Albuquerque, NM, USA 87185
*E-mail address:* Ljsmall@sandia.gov

didate for grid scale storage.

*Keywords:* sodium battery, NaSICON, ion conductor, grid scale, energy storage

## 1. Introduction

The need for large scale, grid-based electrical energy storage continues to become increasingly critical to support a demanding and complex global energy future. For example, in order to integrate intermittent renewable energy such as solar and wind power, large scale battery-based energy storage is needed, allowing use of stored solar energy at night, or stored wind energy on calm days [1, 2, 3]. Additionally, battery storage can provide relief for substations operating near peak capacity, allowing capital-intensive infrastructure upgrades to be delayed for several years or altogether avoided [4]. During large scale emergency response efforts, and as part of national defense activities, safe, reliable electrical energy storage can be a matter of life and death. The diversity of requirements and enormous scale of these applications, makes a suite of different battery chemistries attractive, meeting variable requirements for cost, safety, and scale [5].

To address these growing needs, we describe here a safe, new all inorganic sodium-based energy storage technology that employs a molten sodium anode and a sodium-iodide cathode, separated by a NaSICON solid state separator and operated below 200 °C. Liquid sodium metal is an attractive anode material owing to its high energy density, electrochemical reversibility, high electrical conductivity ($10^5$ S/cm), low melting point (98 °C), and earth abundance [6, 7, 8, 9]. Moreover, liquid metal anodes can avoid dendrite growth issues that plague solid zinc and lithium metals [10]. To this end, several battery chemistries have employed molten sodium anodes, the most notably sodium-sulfur and sodium-nickel chloride (ZEBRA) [11, 12, 13]. While the ZEBRA chemistry avoids some of the challenges of using reactive sodium-sulfur system, both of these technologies traditionally operate at temperatures in excess of 350 °C, well in excess

of sodium's melting temperature. These elevated temperatures increase system complexity, raise operating costs, and introduce problems for long term safety and reliability [10, 14, 15]. Much of the requirement for these high operating temperatures has been dictated by the limited low temperature sodium-ion conductivity of the $\beta$"-$Al_2O_3$ separator traditionally used in these systems [11]. This separator plays several critical roles, providing high sodium ion transport, while isolating the anode and cathode electrically, and preventing unwanted chemical crossover between the two electrodes. The ability to operate at lower temperatures would open the design space for catholyte chemistries, decreasing heating costs, and possibly allowing cell sealing with cost-effective plastics.

## 2. Experimental

### *2.1. Materials*

All active battery materials were kept under dry, inert atmosphere (Ar or $N_2$). Sodium metal (99.8%, Alfa-Aesar) was purified by zone refining. $AlCl_3$ (99%, anhydrous, Alfa-Aesar) was purified via sublimation, avoiding contact with plastic implements. NaI (99+%, anhydrous, Acros Organics) was dried at 350 °C for 3 h and cooled under vacuum before grinding with a mortar and pestle. Carbon electrodes were made from either Super P (LiTICAL graphite & carbon) and Asbury Carbon (A625 SW6581-05) for the 10.0 Ah cell, or graphite felt (SGL GFD4.6) dried at 100 °C overnight on a hotplate under inert atmosphere for the 0.850 and 3.00 Ah cells. Battery casings (304 Stainless steel, McMaster-Carr), tungsten wire (0.009") and tungsten mesh (Unique Wire weaving roll #081405-001) were cut, rinsed in isopropanol and dried in air at 100 °C overnight. The hot materials were directly loaded into the inert atmosphere glovebox and welded as needed.

### *2.2. NaSICON Separator Synthesis*

NaSICON (nominally $Na_3Zr_2Si_2PO_{12}$) tubes were manufactured under proprietary conditions at Ceramatec Corp. NaSICON powder was synthesized

through traditional ceramic powder processing techniques. Stoichiometric ratios of oxides and carbonates were weighed and blended. The resulting powder blend was calcined through solid state reaction techniques and then ball milled to a specific surface area, meeting Ceramatec's internal powder quality control to achieve the final desired microstructure, ionic conductivity, and corrosion resistance to molten sodium when sintered.

The NaSICON powder was spray dried, adding binder and yielding a flowable powder (agglomerates of powder particles), amenable for traditional dry pressing. The spray-dried powder was screened, followed by cold isostatic pressing into tubes, and finally sintering in air to achieve closed porosity (0.00% open porosity, 99.7% theoretical maximum density). All parts were machined to meet final tolerances, and hermeticity checked via helium leak testing.

### *2.3. Battery Assembly*

NaI batteries consisted of four concentric layers: a molten sodium anode (innermost), the NaSICON separator tube, a carbon cathode impregnated with NaI-$ACl_3$ catholyte and wrapped in tungsten wire, and a stainless steel container (outermost) sealed against the NaSICON tube. For the 0.85 and 3.00 Ah cells, graphite felt (CFD4.6, SGL Carbon GmbH, Germany) was placed around the NaSICON tube and tied with tungsten wire. The tungsten wire was welded to the outer stainless steel can. For the 10.0 Ah cell, Super P (LiTICAL graphite & carbon) and Asbury Carbon (A625 SW6581-05) were mixed with powdered NaI and molten NaI-$AlCl_3$. This was manually stirred using an aluminum rod until a consistent slurry was formed. The NaSICON tube was wrapped in tungsten mesh and inserted into the slurry. The tungsten mesh was welded to the outer stainless steel can. Connection to the molten sodium anode was made via a nickel wire hermetically sealed to the NaSICON tube. The active area of the NaSICON tube was defined by the height of molten sodium metal contained during the initial fill.

### *2.4. Characterization*

Electrochemical measurements were recorded using Arbin battery cycler (College Station, TX, USA). Cyclic voltammetry was used to interrogate the electrochemical performance of the NaI-$AlCl_3$ in a standard three electrode cell. The working electrode was the graphite felt, and the reference electrode consisted of sodium metal, and the counter electrode was tungsten mesh.

X-ray diffraction (XRD) was performed with a Bruker D2 Phaser system set in the traditional Bragg-Brentano geometry with Cu K$\alpha$ radiation. NaSICON ceramics were interrogated using a Zeiss Supra 55VP scanning electron microscope (SEM) in backscatter electron imaging mode at 20 kV and 4.4 mm working distance.

Accelerating Rate Calorimetry (ARC, Thermal Hazard Technologies ES ARC System) was used to characterize the heat created during a simulated catastrophic mechanical failure of the NaI battery. In addition to quantification of the heat produced by the reactants, the amount and chemical identity of the gaseous species evolved was determined. (No gas evolution was observed for the NaI-$AlCl_3$ electrolyte). Specific details of system operation are provided elsewhere [16].

## 3. Results and Discussion

The sodium super ion conductor, NaSICON ($Na_{1+x}Zr_2Si_xP_{3-x}O_{12}$), exhibits significantly increased conductivity at temperatures <200 °C. $Na^+$ conductivities as high as 140 mS $cm^{-1}$ have been recorded at 200 °C using a proprietary Ceramatec NaSICON formulation (nominally $Na_3Zr_2Si_2PO_{12}$) from Ceramatec, Inc (Salt Lake City, UT). Still higher ionic conductivities may be achievable with aliovalent doping [17, 18]. In Fig. 1A, the ionic conductivity of Ceramatec NaSICON is compared to that of $\beta$"-$Al_2O_3$; at room temperature several orders of magnitude difference exist in sodium ion conductivity. Critically, this NaSICON is a mechanically robust ceramic separator and is stable against molten sodium [19, 20, 21].

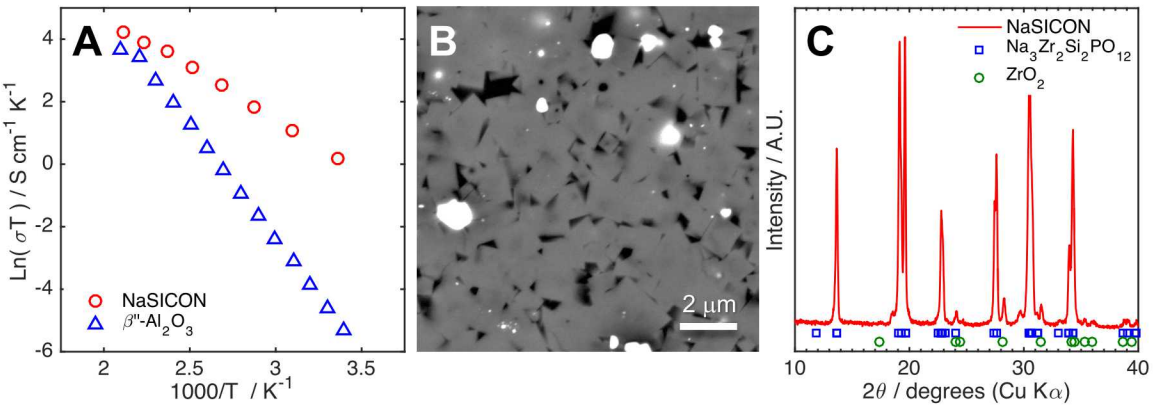


Figure 1: Characterization of the NaSICON separator: (A) Arrenhius plot of $Na^+$ conductivity vs. inverse temperature for Ceramatec NaSICON compared to that of $\beta$"-$Al_2O_3$. (B) Highly-contrasted backscatter SEM micrograph of a polished NaSICON cross section. (C) X-ray diffraction (Cu K$\alpha$ radiation) patterns for Ceramatec NaSICON compared to peak positions for $Na_3Zr_2Si_2PO_{12}$ and $ZrO_2$ (PDF# 04-008-8579 and 01-083-0943).

The ability to create a dense NaSICON tube is not trivial, though through liquid phase sintering a 99.7% dense microstructure can be achieved, as seen in the SEM micrograph of Ceramatec NaSICON in Fig. 1B. Here smooth-faceted grains approximately 1 $\mu$m in diameter are observed, with a glassy region between grains. Due to the highly-contrasted SEM backscatter electron image, the glassy regions between NaSICON grains appear dark; this is not porosity. Bright spots correspond to a slight $ZrO_2$ impurity, corroborated by X-ray diffraction analysis of the sample (Fig. 1C). Typically processed at temperatures between 900-1300 °C, NaSICON also represents a potentially significant manufacturing advantage over other materials such as $\beta$"-alumina, which requires processing temperatures in excess of 1450 °C to create structures of similar size and mechanical integrity [22, 23].

A recent report from Ceramatec and SK-Innovation has shown that traditional ZEBRA battery performance may be improved by additives stable only at the lower temperatures enabled by a NaSICON separator [21]. We believe even higher efficiencies and greater battery lifetimes may be achieved, however,

if the redox active species are soluble in the electrolyte. This is in stark contrast to most battery chemistries which involve intercalation and/or plating of solid metals (Li, Zn, Ni, etc.) where the huge strains and/or particle ripening limit effective battery lifetimes [21, 24, 25].

Although the molten metallic sodium makes a convenient and simple anode and current collector in this system, the cathode is slightly more complex. The 50:50 at% NaI-$AlCl_3$ molten catholyte has a solidus melting temperature near 95 °C, quite close to sodium's melting temperature. These low melting temperature molten components allow for 120-180 °C operating temperatures. Recent works have shown $I^-$ admirable for its high energy density, and molten salts enviable for their unreactivity towards molten sodium [26, 27, 28, 29]. Further, the redox-active $I^-$ is present throughout the molten salt at very high concentrations (≈11 M), which would be expected to yield a high energy density and rapid reaction kinetics, analogous to using high iodide concentrations in water (≈12 M) [27]. Interrogation of the NaI-$AlCl_3$ system lead us to identification of NaI-$AlCl_3$ (60:40 at%) as a choice electrolyte. Here the NaI-$AlCl_3$ solution is saturated with about 5-10 at% excess NaI, depending on temperature. In Fig. 2A, cyclic voltammetric (CV) analysis of the molten salt at a carbon felt electrode shows facile iodide oxidation and triioidide reduction near 2.9 V vs. $Na/Na^+$. $Al^{3+}$ reduction resides >1 V below triodide reduction, providing ample room for electrode polarization without plating aluminum metal from the electrolyte. The electrical conductivity of the NaI-$AlCl_3$ (60:40 at%) electrolyte was evaluated as a function of temperature; conductivities were found to be greater than those of the NaSICON electrolyte, as plotted in Fig 2B. Thus, the ionic conductivity of the electrolyte should not hinder overall cell performance, as these conductivities approach the conductivity of KOH or $H_2SO_4$-based electrolytes found in widely used alkaline and lead-acid batteries, respectively [30, 31].

Having identified an anolyte, separator, and catholyte, a series of cells were assembled. Although other studies have recently described promising results in low-to-intermediate temperature systems using $\beta$"-alumina (8), these systems were on a very small scale (<0.5 Ah) and the low conductivity of the alumina

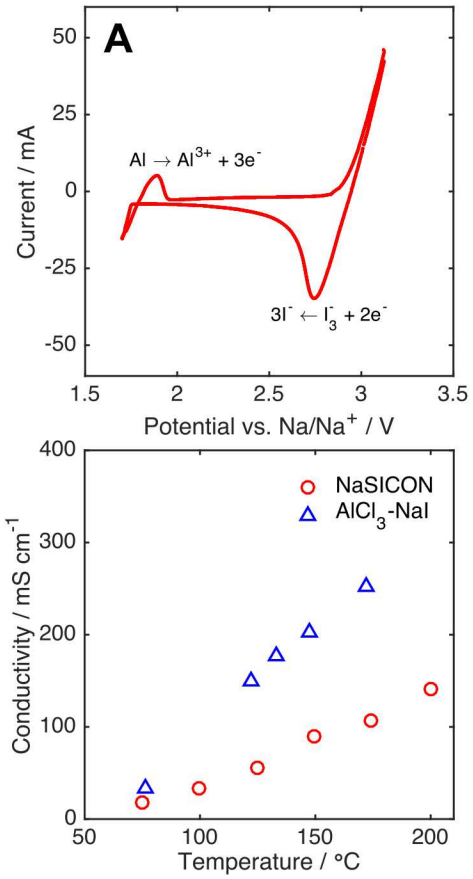


Figure 2: (A) CV of a carbon felt electrode in the $AlCl_3$:NaI (40:60 at%) catholyte at 125 °C and 100 mV $s^{-1}$. (B) Ionic conductivity of the $AlCl_3$:NaI catholyte and Ceramatec NaSICON as a function of temperature.

separators necessitated specialized, thin (<600 $\mu$m) geometries to obtain 10 mA $cm^{-2}$. Here, the high inherent conductivity and robust mechanical character of the NaSICON separator allows us to apply up to 50 mA $cm^{-2}$ across robust 1.5 mm thick NaSICON. Here we describe gradually increasing the cell format from 0.85 Ah to 3 Ah, and then 10 Ah. The basic cell design consisted of four concentric layers: (innermost) the liquid sodium anode, a closed-end Ceramatec NaSICON tube, the NaI-saturated NaI-$AlCl_3$ (60:40 at%) catholyte and carbon

felt electrode, and an alumina-lined stainless steel can welded shut (outermost). A photograph of the 10 Ah prototype battery and a cross sectional schematic are shown in Figs. 3A-B. Fundamentally, the ideal chemical reactions, depicted in Fig. 3C, at the anode and cathode upon discharge at standard state may be written as follows, where "$E^0$" is the standard state potential [32]:

$$Na \rightarrow Na^+ + e^-,\ E^0 = 0\ \text{V vs. Na/Na}^+ \quad (1)$$

$$I_3^- + 2e^- \rightarrow 3I^-,\ E^0 = 3.24\ \text{V vs. Na/Na}^+ \quad (2)$$

$$2Na + I_3^- \rightarrow 2Na^+ + 3I^-\quad E^0_{\text{cell}} = 3.24\ \text{V} \quad (3)$$

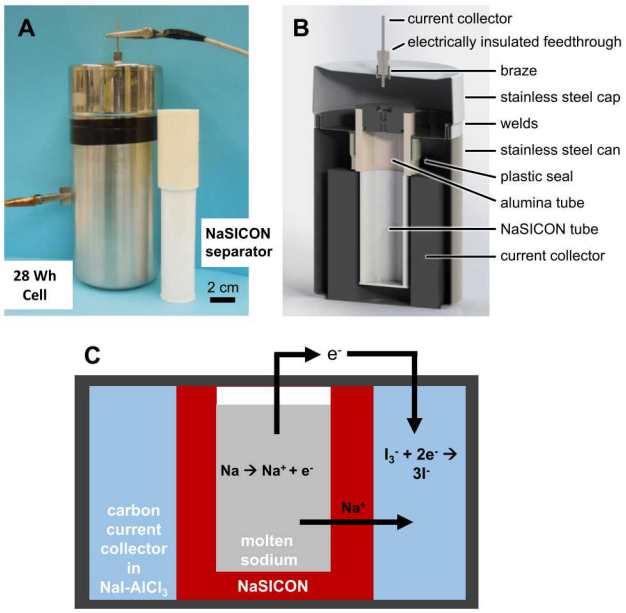


Figure 3: (A) Photograph of prototype 28 Wh (10 Ah) NaI battery assembly with NaSICON separator at right. (B) 3D model of the 28 Wh NaI battery assembly. (C) Schematic of battery (not to scale) depicting chemical reactions and ion movement upon battery discharge.

The open circuit potentials of an assembled battery (fully discharged) typically read 2.80-2.90 V, consistent with deviations from standard state expected for actual battery operating conditions. Once assembled, the 0.850 Ah cell was

heated to 150 °C and put through several conditioning cycles before cycling at C/11, as shown in Fig. 4A. The discharge rate was then gradually increased to C/5, and backed off to C/11 and C/7 for the final cycles. While the voltage efficiency (VE) decreases with increasing discharge rate, the Coulombic efficiency (CE) is nominally unaffected, averaging to 99.45%. Nevertheless, the lifetime energy efficiency (EE) was recorded at 81.96%, with an EE of 84.65% at C/11. EE was calculated as the product of the CE and VE. The lifetime average efficiencies for each cell plotted in Fig. 4 have been compiled in Table 1.

| Cell Size / Ah | Run time / h | CE / % | VE / % | EE / % |
|---|---|---|---|---|
| 0.850 | 1032 | 99.45 | 82.41 | 81.96 |
| 3.00 | 3024 | 95.34 | 84.64 | 80.67 |
| 10.0 | 1022 | 99.05 | 77.21 | 76.60 |

Table 1: Lifetime average performance of NaI cells presented in this work. All values are averages and exclude initial conditioning cycles.

Performance results from a 3 Ah cell run in excess of 3000 h (4 months) are shown in Fig. 4B. Here EE in excess of 80% are observed for nearly all cycles, despite varied temperature and discharge rates. After 130 cycles, the cell was cooled to room temperature for 1 week, before reheating and more cycling. While the CE generally follows the same trend as before cooling (after the initial few cycles), the VE stabilizes near 86%. Overall superior performance is observed at 180 °C and consistent cycling at C/7 for cycles number 150-250, with 94.18% CE, 86.26% VE, and 81.25% EE.

An even larger cell was assembled at 10.0 Ah size. Over 1000 h of testing at C/7 CE averaged in excess of 99%, while the VE hovered around 77%. At such a large scale, creating a uniform salt composition throughout the catholyte is a potential concern. As the battery is charged, $Na^+$ are driven from the catholyte into the molten sodium anode, decreasing the $Na^+$ concentration in the catholyte until the excess NaI in the catholyte fully dissolves. In order to ensure a uniform distribution of excess NaI, a C/15 charge and discharge every 11th cycle was employed, resulting in the best performing 10 Ah cells.

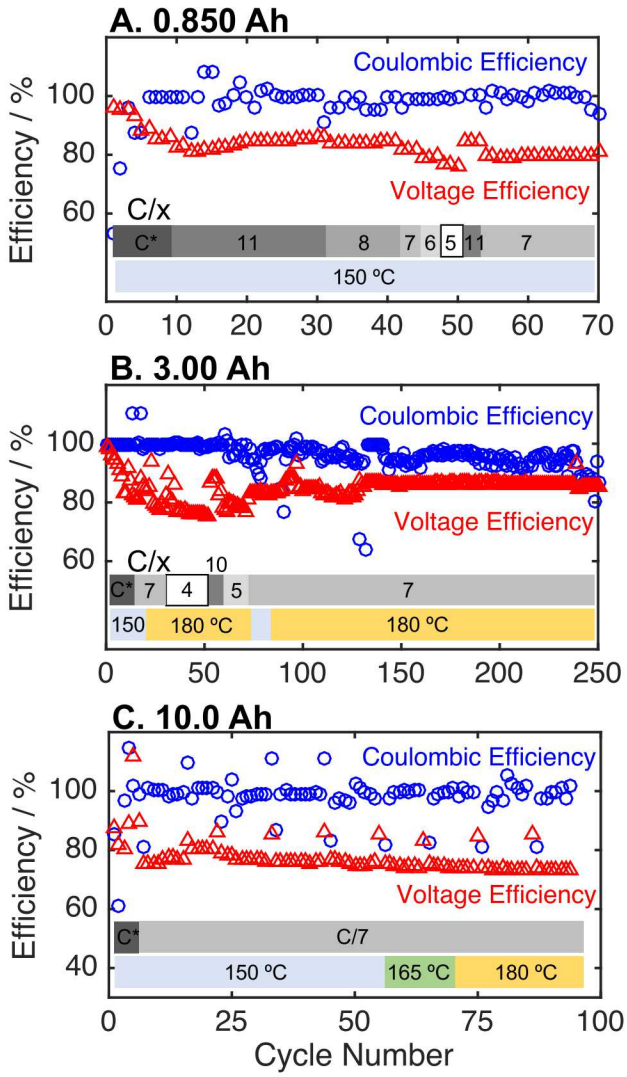


Figure 4: Coulombic efficiency, voltage efficiency, operating temperature, and discharge rate for NaI batteries of different sizes (A) 0.850 Ah, (B) 3.00 Ah, (C) 10.0 Ah. For (C) every 11th cycle is at C/15. "C*" Indicates a series of initial conditioning steps at low rates.

This change in C-rate is evidenced in Fig. 4C, where every 11th cycle an artificial increase in Coulombic efficiency is seen, followed by an artificially lower Coulombic efficiency upon return to C/7. Here the same voltage limits were

maintained, regardless of cycling rate. As expected, the lower C-rate improved the VE at these cycles due to decreased IR losses inherent to smaller currents. Higher VEs are also likely due to a more uniform concentration of $I^-$ vs. $I_3^-$ throughout the bulk electrolyte and electrode surface. It is reasoned that the decreased rate facilitates a more uniform catholyte by allowing more time for diffusion to homogenize compositional variations. Future improvements to the carbon collector may improve catholyte compositional uniformity and electrical conductivity, both expected to improve both VE and EE.

Importantly, if cooled to room temperature, then reheated, the performance of these cells does not deteriorate. After more than 2 months (130 cycles), the 3 Ah cell in Fig. 3B was cooled to room temperature and allowed to sit for a week before reheating to 180 °C and testing resumed. The repeatability of the voltage profile at C/7 before and after cooling is shown in Fig. 5A. Furthermore, consistent performance is observed for varying depths of discharge. At C/7, the charge profiles for the 3 Ah cell overlay tightly when increasing from 50% state of charge (1.5 Ah capacity) to 90% state of charge (2.7 Ah capacity), as shown in Fig. 5B. Slight decreases in the discharging profile correspond to a slight decrease from 80% EE to 76% EE.

Alternative batteries under consideration for grid-scale storage, such as Li-ion or sodium-sulfur, perform effectively under standard operating conditions. The inherent nature of the chemistries in these systems introduce hazardous, reactive components, and makes them inherently intolerant to significant mechanical or thermal stress, potentially leading to catastrophic, cascading failures [33, 34, 35]. These concerns are particularly important for grid scale systems, where MWh capacities represent potentially dangerous amounts of stored energy. Separator failure or internal short-circuits in these systems can lead to uncontrolled reactions, exothermic runaway, and overpressurization of flammable or toxic gases, all of which make these systems susceptible to hazardous, chain-reaction fires. In contrast, the chemistry of the current system is inherently less dangerous than these other systems. To demonstrate this improved safety, sodium metal was mixed at room temperature with the NaI-$AlCl_3$

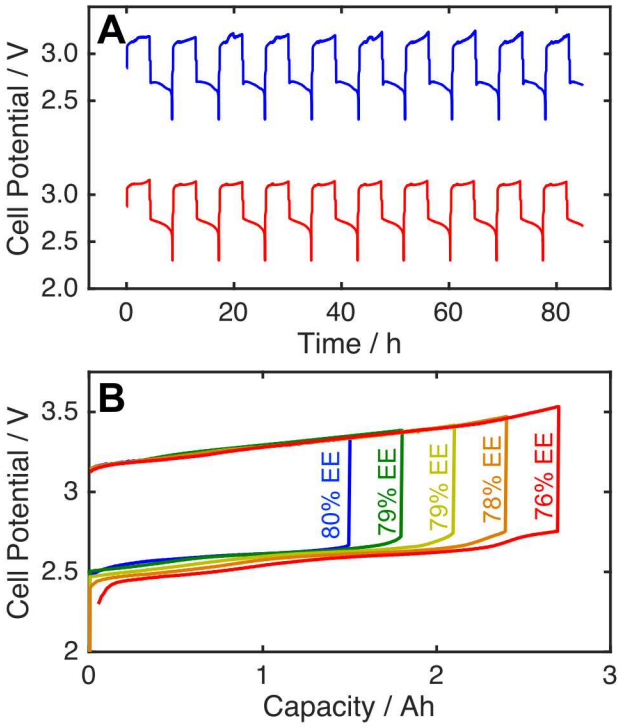


Figure 5: (A) 3 Ah cell voltage profiles at C/7, 180 °C before (upper, blue) and after (lower, red) idling for 1 week at room temperature. (B) Influence of depth of discharge on the charge-discharge curves and EE of the 3 Ah cell at 150 °C and C/7.

catholyte used in this system and tested using an accelerated rate calorimeteter, commonly used to assess thermal runaway and system pressurization in Li-ion systems. When heated from room temperature to 400 °C, the reagents melted, allowing intimate contact between the anode and cathode in a simulation of complete separator failure. Throughout this test, however, there was no significant exotherm measured and, as shown in Fig. 6, there was no generation of pressurizing gas. In fact, Fig. 6 compares the undetectable gas evolution of the NaI-$AlCl_3$ electrolyte (mixed with 1 molar equivalent sodium metal) to the significant pressure generated by a Li-ion electrolyte composed of ethylene carbonate (EC) ethyl methyl carbonate (EMC) electrolyte (3:7 EC:EMC) with 1.2 M $LiPF_6$. For this commonly used Li-ion battery electrolyte, gases $H_2$, CO,

and $CH_4$ are generated in measurable quantities, representing a potential fire and explosion hazard [16]. The safety of the NaI battery chemistry, in terms of heat and gas production upon mechanical failure, surpasses that of many Li-ion chemistries and intrinsically hazardous Na-aqueous chemistries proposed in the literature [26, 16, 36]. Moreover, the ultimate byproducts of the Na/NaI-$AlCl_3$ mixture are non-hazardous aluminum metal and NaCl, meaning that this system not only fails to generate hazardous thermal runaway and fire hazards, but the byproducts of the failed system do not add any additional hazards. Overall, this system represents a significant advance in battery safety through the inherently safe nature of the battery chemistry.

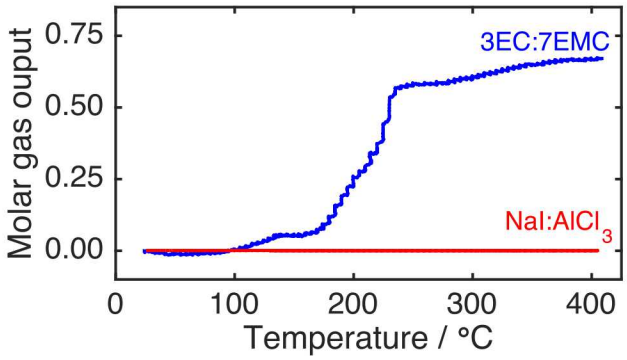


Figure 6: Molar gas output (moles of gas produced per moles of electrolyte) for the NaI-$AlCl_3$ electrolyte of the NaI battery compared to a standard Li-ion electrolyte, 1.2 M $LiPF_6$ in EC:EMC (3:7).

## 4. Conclusion

We have demonstrated the viability of an innovative NaI-based battery which operates near 150 °C with lifetime average CE as high as 99.45% and EE of 81.96% over dynamic testing lasting ¿3000 hours. Further improvements in cathode design will further increase energy efficiencies. This energy dense, readily scalable battery consists only of earth-abundant materials, making it an economically attractive system for grid scale storage. Moreover, the anolyte and

catholyte chemistries contained within this system introduce inherent safety in the event of battery failure, mitigating concerns of cascading thermal runaway, flammability or production of hazardous byproducts. The promising performance of these prototypes across several lab-scale capacities promises opportunities to develop this new technology into a viable and important technology for future energy storage.

## 5. Acknowledgements

The authors thank Mr. C. Taylor and Ms. B. McKenzie for preparing and recording SEM micrographs of NaSICON samples. This work was generously supported by program manager Dr. Imre Gyuk through the U.S. Department of Energy, Office of Electricity Delivery and Energy Reliability. Sandia National Laboratories is a multi-mission laboratory managed and operated by National Technology and Engineering Solutions of Sandia, LLC, a wholly-owned subsidiary of Honeywell International, Inc., for the U.S. Department of Energy's National Nuclear Security Administration under contract DE-NA0003525.

## References

[1] J. Goodenough, Electrochemical energy storage in a sustainable modern society, Energy Environ. Sci. 7 (2014) 14–18.

[2] W. Pickard, D. Abbott, Addressing the intermittency challenge: massive energy storage in a sustainable future, P. IEEE 100 (2012) 317–321.

[3] Z. Yang, J. Zhang, M. Kintner-Meyer, X. Lu, D. Choi, J. Lemmon, J. Liu, Electrochemical energy storage for green grid, Chem. Rev. 111 (2011) 3577–3613.

[4] R. Talbot, Energy storage: A utility perspective, New Mexico Regional Energy Storage and Grid Integration Workshop, 2016.

[5] B. Dunn, H. Kamath, J.-M. Tarascon, Electrical energy storage for the grid: a battery of choices, Science 334 (2011) 928–935.

[6] S. Ha, J.-K. Kim, A. Choi, Y. Kim, K. Lee, Sodium-metal halide and sodium-air batteries, ChemPhysChem 15 (2014) 1971–1982.

[7] K. Hueso, M. Armand, T. Rojo, High temperature sodium batteries: status, challenges and future trends, Energy Environ. Sci. 6 (2013) 734–749.

[8] W.-L. Pang and X.-H. Zhang and J.-Z. Gou and J.-Y. Li and X. Yan and B.-H. Hou and H.-Y. Guan and X.-L. Wu, P2-type $Na_{2/3}Mn_{1-x}Al_xO_2$ cathode material for sodium-ion batteries: Al-doped enhanced electrochemical properties and studies on the electrode kinetics, J. Power Sources 356 (2017) 80–88.

[9] F. Wan ad X.-L. Wu and J.-Z. Gou and J.-Y. Li and J.-P. Zhang and L. Niu and R.-S. Wang, Nanoeffects promote the electrochemical properties of organic $Na_2C_8H_4O_4$ as anode material for sodium-ion batteries, Nano Energy 13 (2015) 450–457.

[10] X. Lu, G. Li, J. Kim, D. Mei, J. Lemmon, V. Sprenkle, J. Liu, Liquid-metal electrode to enable ultra-low temperature sodium-beta alumina batteries for renewable energy storage, Nat. Commun. 5 (2014) 4578.

[11] J. Sudworth, The sodium/nickel chloride (zebra) battery, J. Power Sources 100 (2001) 149–163.

[12] K. Hueso, V. Palomares, G. Singh, M. Armand, T. Rojo, Handbook of clean energy systems, Wiley, 2015.

[13] J. Kummer, N. Weber, Sae technical paper 670179doi:10.4271/670179.

[14] J. Ohi, Environmental, Health, and safety issues of sodium-sulfur batteries for electric and hybrid vehicles, Vol. 1 Cell and Battery Safety, NREL, 1992.

[15] S. Xin and Y.-X. Yin and Y.-G. Guo and L.-J. Wan, A High-Energy Room-Temperature Sodium-Sulfur Battery, Adv. Mater. 26 (2014) 1261–1265.

[16] J. Lamb, C. Orendorff, E. Roth, J. Langendorf, Studies on the thermal breakdown of common li-ion battery electrolyte components, J. Electrochem. Soc. 162 (2015) A2131–A2135.

[17] A. Jolley, G. Cohn, G. Hitz, E. Wachsman, Improving the ionic conductivity of nasicon through aliovalent cation substitution of $na_3zr_2si_2po_{12}$, Ionics 21 (2015) 3031–3038.

[18] A. Jolley, D. Taylor, N. Schreiber, E. Wachsman, Structural investigation of monoclinic-rhombohedral phase transition in $na_3zr_2si_2po_{12}$ and doped nasicon, J. Amer. Ceram. Soc. 98 (2015) 2902–2907.

[19] X. Lu, G. Xia, J. Lemmon, Z. Yang, Advanced materials for sodium-beta alumina batteries: status, challenges and perspectives, J. Power Sources 195 (2010) 2431–2442.

[20] X. Lu, G. Li, J. Kim, J. Lemmon, V. Sprenkle, Z. Yang, The effects of temperature on the electrochemical performance of sodium-nickel chloride batteries, J. Power Sources 215 (2012) 288–295.

[21] J. Kim, S. Jo, S. Bhavaraju, A. Eccleston, S. Kang, Low temperature performance of sodium-nickel chloride batteries with nasicon electrolyte, J. Electroanal. Chem. 759 (2015) 201–206.

[22] N. Bell, C. Edney, J. Wheeler, D. Ingersoll, E. Spoerke, The influences of excess sodium on low-temperature nasicon synthesis, J. Amer. Ceram. Soc. 97 (2014) 3744–3748.

[23] J. Ihlefeld, E. Gurniak, B. Jones, D. Wheeler, M. Rodriguez, A. McDaniel, Preparation and processing temperature effects on ion conductivity in solution derived sodium zirconium phosphate ($nazr_2p_3o_{12}$) thin films, J. Electrochem. Soc. 161 (2014) A364–A367.

[24] V. Etacheri, R. Marom, R. Elazari, G. Salitra, D. Aurbach, Challenges in the development of advanced li-ion batteries: a review, Energy Environ. Sci. 4 (2011) 3243–3262.

[25] F. McLarnon, E. Cairns, The secondary alkaline zinc electrode, J. Electrochem. Soc. 138 (1991) 645–656.

[26] Y. Zhao, L. Wang, R. Byon, High-performance rechargeable lithium-iodine batteries using triiodide/iodide redox couples in an aqueous cathode, Nat. Commun. 4 (2013) 1896.

[27] X. Dong, L. Chen, J. Liu, S. Haller, Y. Wang, Y. Xia, Environmentally-friendly aqueous li (or na)-ion battery with fast electrode kinetics and super-long life, Sci. Adv. 2 (2016) e1501038.

[28] L. Xue, T. Tucker, C. Angell, Ionic liquid catholyte for high energy efficiency, low-cost energy storage, Adv. Energ. Mater. 5 (2015) 1500271.

[29] Q. Huang, J. Yang, C. Ng, C. Jia, Q. Wang, A redox flow battery based on the redox targeting reaction between lifepo4 and iodide, Energy Environ. Sci. 9 (2016) 917–921.

[30] R. Gilliam, J. Graydon, D. Kirk, S. Thorpe, A review of specific conductivities of potassium hydroxide solutions for various concentrations and temperatures, Int. J. Hydrogen Energ. 32 (2007) 359–364.

[31] T. Compton, Battery Reference Book, 3rd Edition, Newnes, 2000.

[32] A. Bard, L. Faulkner, Electrochemical Methods: Fundamentals and Applications, 2nd Edition, Wiley, 2000.

[33] Q. Wang, P. Ping, X. Zhao, G. Chu, J. Sun, C. Chen, Thermal runaway caused fire and explosion of lithium ion battery, J. Power Sources 208 (2012) 210–224.

[34] J. Zhang, J. Lee, A review on prognostics and health monitoring of li-ion battery, J. Power Sources 196 (2011) 6007–6014.

[35] P. Balakrishnan, R. Ramesh, T. Kumar, ,safety mechansims in lithium-ion batteries, J. Power Sources 155 (2006) 401–414.

[36] C. Liu, J. Shamie, L. Shaw, V. Sprenkle, An ambient temperature molten sodium-vanadium battery with aqueous flowing catholyte, ACS Appl. Mater. Inter. 8 (2016) 1545–1552.